ADVANCED OPTICAL MATERIALS
www.advopticalmat.de

First-Principles Calculations of Quantum Efficiency for Point Defects in Semiconductors: The Example of Yellow Luminance by GaN: C_N+O_N and GaN:C_N

Hai-Shan Zhang, Lin Shi, Xiao-Bao Yang, Yu-Jun Zhao, Ke Xu, and Lin-Wang Wang**

Point defects play an important role in the photoelectrical properties of semiconductor materials, and they can be luminescence centers. However, the relationships among the observed luminescence wavelengths, intensities, and the microscopic processes are in most cases unknown, or depend heavily on parameter fitting. In this work, the light-emitting quantum efficiencies for point defects using ab initio density functional theory are calculated. The study of radiation recombination for electrons and nonradiation recombination for holes is reported here. The results show that the defect C_N transition between "–" and "0" charged levels and the defect C_N+O_N transition between "0" and "+" charged levels both may be responsible for the yellow luminescence (YL) which is observed in experiment. Moreover, the calculation shows significant thermal quenching of the YL starting at 480 K due to re-excitation of hole into the valence band from the point defects, which is in relatively good agreement with the experimentally observed value. This work shows that it is possible to use ab initio calculations to understand the microscopic mechanisms and the competitions among different channels for the light emissions caused by defects.

GaN is an important third-generation optoelectronic semiconductor which has attracted much attention in recent years owing to its large direct band gap,[1–3] high thermal conductivity,[4] and high breakdown voltage.[5] Many works have focused on understanding the origin of the luminescence phenomena (e.g., red, yellow, green, and blue luminescence) in unintentionally doped GaN.[6–21] For the YL, which was ascribed to the electron transition from CBM or shallow donor to deep acceptor. Carbon and oxygen impurities will always be introduced unintentionally during the samples preparation process. Since 1980, Toshio and other researchers reported that carbon, oxygen impurities, and gallium vacancy may be responsible for the emission (YL) with a maximum at 2.2 eV in undoped GaN.[7,12,18,22,23] Furthermore, some researchers have reported that the YL intensity increases with the increasing carbon concentration by a constant amount of oxygen.[19] Depending on the growth techniques and growth conditions, the concentrations can range from 10^{15} to 10^{18} cm^{-3} (C)[18,19] and 10^{16} to 10^{17} cm^{-3} (O)[18,19] in the samples containing YL band. Nevertheless, the exact defects and their transition states responsible for this YL are still under debate. In addition, the quantum efficiencies (QE) of the defect luminescence have been extensively studied in experiment,[9,24,25] but a quantitative comparison between the experimental data and parameter free theoretical calculation is yet to be achieved. Clearly, the control of point defects is extremely important in modifying the photoelectrical properties of semiconductor materials. Therefore, to map out the relationship between macroscopic phenomena and the microscopic point defect origin and its process is the key for photoelectric material design and material improvement. However, it is difficult to directly identify the microscopic mechanism using today's experimental optical spectroscopic measurements, despite the existence of abundant experimental data. Very often, models are used with heavy parameter fitting to explain the experimental results. Such practice is extremely useful and has yield significant understanding of the microscopic processes. Nevertheless, it will be much more desirable if pure ab initio calculation can be used to explain the experimental results without parameter fitting.

In the past few decades, density functional theory (DFT) has become a powerful method to evaluate the structures, and as well as formation energies of point defects. As the calculation method progresses, Heyd–Scuseria–Ernzerhof (HSE) hybrid density functional theory[26] was employed to achieve accurate electronic structure results.[14,16,18,25,27,28] The calculated band gaps of GaN are in agreement with the experimental data (3.50 eV).[2,3] Based on such calculations, it could

H.-S. Zhang, Prof. L. Shi, Prof. K. Xu
Suzhou Institute of Nano-Tech and Nano-Bionics
Chinese Academy of Sciences
Suzhou 215123, P. R. China
E-mail: lshi2007@sinano.ac.cn

H.-S. Zhang, Prof. X.-B. Yang, Prof. Y.-J. Zhao
Department of Physics and Key Laboratory of Advanced
Energy Storage Materials of Guangdong Province
South China University of Technology
Guangzhou 510640, P. R. China

Prof. K. Xu
Suzhou Nanowin Science and Technology Co., Ltd.
Suzhou 215123, P. R. China

Prof. L.-W. Wang
Materials Sciences Division
Lawrence Berkeley National Laboratory
One Cyclotron Road, Mail Stop 66, Berkeley, CA 94720, USA
E-mail: lwwang@lbl.gov

DOI: 10.1002/adom.201700404

© 2017 WILEY-VCH Verlag GmbH & Co. KGaA, Weinheim

be very helpful to have ab initio calculations to directly explain the experimental optical measurements. Van de Walle and coworkers employed 1D quantum formula to calculate the nonradiative recombination (non-RR) coefficient of point defect C_N in GaN.[17] But the calculated coefficient could be significantly smaller than the fitted value of experiment. Our previous studies revealed that, comparing with other formalisms, static coupling theory can provide a more accurate result for the non-RR in point defects of III–V compounds.[29,30] However, a complete deep-level photoluminescence process consists of two parts: radiative recombination (RR) and non-RR. Due to their competitions, it is insufficient to consider only the non-RR when compared with experiments, especially for the luminescence intensity. It is necessary to consider all the major processes and channels, then solve the steady-state results due to the balance of different channels. In the current work, we take the defects in GaN as an example to illustrate this approach. Nevertheless, it is still too complicated to take into all the possible channels purely ab initially given all the uncertainties in the system. Instead, we will combine ab initio calculation with some experimental data, and use that to explain other experimental data. In particular, we will use the measured band edge photoemission to obtain the information of band edge hole carrier density in the system, then use this density to calculate the non-RR of the hole and RR of the electron to a single defect to determine the PL due to this defect. This significantly enhances the reliability of the approach, and also provides a platform to test the ab initio method and confirm the hypothesis of the microscopic defect center for an experimentally identified PL peak. In this work, we will focus on the YL band in the optical measurement.

Using the HSE hybrid function, some researchers have concluded that the point defect C_N acts as the deep acceptor,[14,16,17] and that may induce YL band in undoped GaN. However, recently Reshchikov's group reported that, in contrast to the isolated defect C_N, the C_N+O_N defect complex is energetically more favorable to be formed, and its calculated optical properties, such as photoabsorption (PA) and photoluminescence (PL), a zero phonon line (ZPL), and the thermodynamic transition level (ΔE), all agree excellently with measured YL data.[16] They also studied the temperature dependence of the photoluminescence in undoped GaN films.[9] Nevertheless, the key parameters: RR coefficient (C_n) and non-RR coefficient (C_p) are obtained by fitting, instead of calculating theoretically. Furthermore, some assumptions used in the fitting procedure could be questionable. For example, the fitted C_p parameter was kept as a constant, independent of temperature, which might not be a good assumption as will be shown below. To solve the issue of C_N versus C_N+O_N for the origin of YL (they have very close energy levels, both consistent with experiment), we like to go beyond the energy level comparison with the experiment. We will include the non-RR and RR dynamics. We also go beyond the phenomenological fitting of ref. [9] by using purely ab initio calculations.

We introduce the formation energy calculations of (C, O)-related defects based on first-principle calculations and compare the transition energies with experimental observations. We give a detail derivation of defect-related luminescence quantum efficiency (QE) formalism in the presence of several defects at an arbitrary temperature. The computational procedures of RR coefficient (C_n) and non-RR coefficient (C_p) are presented in this study. For the hole capture process, we adopt a "scaling factor" correction to describe the Coulomb attraction between C_N^- and holes. The result and discussion of this work are presented. At 480 K, the calculated YL begin to quench significantly, and the quenching mechanism will be discussed.

The crystal structure optimizations were performed by using the Vienna ab initio simulation package(VASP) code.[31,32] We have also used PWmat[33,34] to make self-consistent field (SCF) calculations, to obtain the force constant matrixes, phonon density of states (PDOS), and electron–phonon coupling coefficient ($C_{i,j}^k$). A 128-atom ($4 \times 4 \times 2$) supercell is used to calculate the formation energies of (C, O)-related defects by VASP code. Both the undoped and doped GaN atomic structures were optimized by using the screened hybrid functional of HSE.[35] In this work, the mixing parameter (α) of HSE was set to 0.30. A kinetic energy cutoff of 450 eV was used in all calculations. The relaxed lattice parameters of primitive cell, a = 3.21 Å, c = 5.21 Å, u = 0.377 Å, are in good agreement with the experimental results at room temperatures (a = 3.19 Å, c = 5.19 Å, and u = 0.377).[36] Following ref. [37], the formation energy of C, O-related defects ΔE^q are calculated and shown in **Figure 1**. Here, we study the N-poor and N-rich experiment conditions. In either case, the O substituting on the N site (O_N) acts as a shallow donor and has a quite low formation energy, and that may be the reason why the unintentionally doped GaN is an n-type semiconductor. As shown in Figure 1, our calculated −/0 and 0/+ transition energies of defect C substituting on the N site (C_N) are at 0.79 and 0.50 eV above the valence band maximum (VBM), respectively, which are in good agreement with the theoretically calculated values in other works.[14,18,27] Since the predominant tendency to form O_N as shown in Figure 1, and all the experimental evidence for the existence of C_N defect, it is safe to assume both O_N and C_N coexist in the GaN. The calculated 0/+ transition level of the defect complex C_N+O_N is located at 0.76 eV above the VBM, which is in agreement with the previous computed results.[16] The experimental value obtained from quenching of YL at high temperature is 0.81 eV,[9] which is consistent with our calculated 0.79 eV (for C_N) and 0.76 eV (for C_N+O_N). Correcting the possible error from thermal quenching experiment, the defect energy level was estimated at 0.85 eV in refs. [7,16]. Furthermore, the low-temperature ionization energy determined from the observed zero-phonon line for the YL band is 0.916 eV,[21] which is slightly larger than the room-temperature results and our calculated results. However, since the calculated lattice constant is closer to high-temperature experimental values than low-temperature values, it might be appropriate to use our calculated energy levels to represent the high-temperature experimental results. One can also deduce the formation energy of forming a neutral C_N+O_N pair from two separate neutral C_N and O_N centers from Figure 1. This formation energy is huge, 2.6 eV. Thus, as concluded in refs. [16,18], it seems very likely to form the C_N+O_N donor–acceptor pair. Nevertheless, the defect formation energy sensitively depends on the values of the chemical potentials. Different chemical potentials can produce very different results. In ref. [27], under the n-type condition, for example, with E_F higher than 2.4 eV, it is concluded that the C_N defect

© 2017 WILEY-VCH Verlag GmbH & Co. KGaA, Weinheim

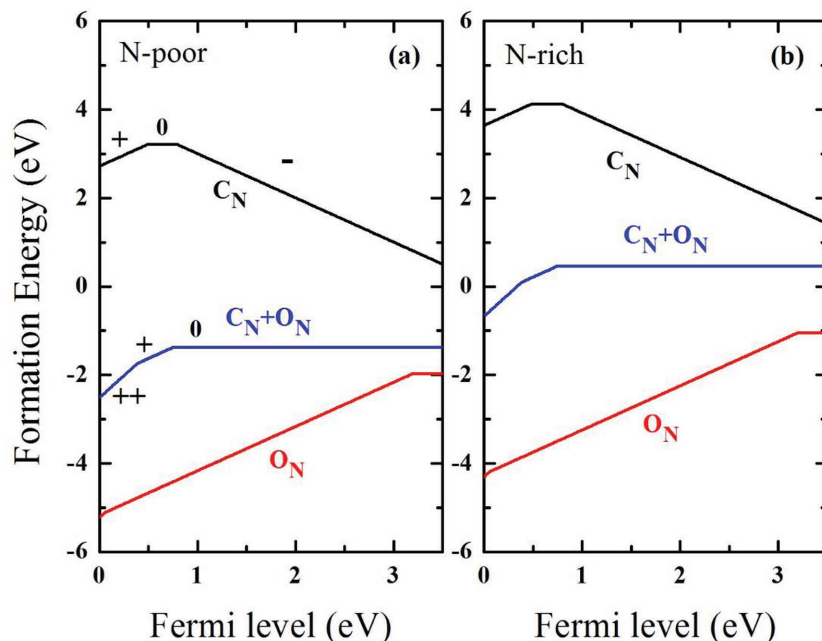

Figure 1. The defect formation energies of C_N, O_N, and C_N+O_N as a function of Fermi level at different charge states in N-rich and N-poor growth conditions.

can have lower formation energy than the C_N+O_N complex. As a result, both C_N+O_N and C_N could be presented in the system, much depends on the synthesis condition. Furthermore, as will be discussed below, the energy levels of these two defects are very similar, thus it will be difficult to distinguish them from the pure energy comparison with the PL energy. However, their charge states are different. As shown in Figure 1, in n-type GaN, the ground states of defects C_N+O_N and C_N are "0" charge state and "–" charge state, respectively. Their excited states are "+" charge state and "0" charge state, respectively. Such charge difference causes some difference in their dynamics. The configuration coordinate diagram of **Figure 2** shows a series of defect-related photophysical processes. Within the Franck–Condon approximation, the abscissa Q is used to represent the atomic configuration. PA is an excited process from ground state to excited state, PL is a de-excited process from excited state to ground state and ZPL energy is the difference between the band gap energy and the transition energy. d_{FC}^{g} is the lost energy in this process of the atomic configuration which relaxes from equilibrium Q value of excited state to the equilibrium Q value of ground state (Figure 2). From first principles, the calculated PA, PL, and ZPL energies are 3.11 eV (E_{PA}), 2.23 eV (E_{PL}), and 2.74 eV (E_{ZPL}) for defect complex C_N+O_N and 3.01 eV (E_{PA}), 2.16 eV (E_{PL}), and 2.71 eV (E_{ZPL}) for defect C_N. These energies between C_N+O_N and C_N are close. As shown in **Table 1**, our results are in good agreement the theoretical calculating values of other works.[14,16,18,27] Comparing the DFT calculation results with the experimental values,[7] due to the possible errors of the former, we think both of these defects could be responsible for the YL in experiment. Hereafter, we call the $(C_N+O_N)^{0/+}$ as YL1 and $C_N^{-/0}$ as YL2. We will calculate the quantum efficiencies of both of these two suspected defects, and try to distinguish them from their PL intensity and dynamics.

As shown in **Figure 3**, under a photoexcitation, the nonequilibrium electron–hole pairs would be generated and the carrier generation rate can be expressed as G. We will describe the continuous photoexcitation processes. Thus, everything is in equilibrium under this condition. In the n-type system, the hole is the minority carrier. Under the optical excitation, the recombination process of the free carrier is expressed as process-a. We will consider relatively high temperature, thus we can ignore the exciton formation and its process.

The recombination processes related to YL1 $(C_N+O_N)^{0/+}$ and YL2 $(C_N^{-/0})$ as shown in Figure 3 include: a hole transition from VBM to the defect level (process-b and e) and an electron transition from CBM to ionized defect level (process-c and f). In addition, there are two reverse processes related to the above processes: the re-excitation of the hole from the defect to the VBM (process-d and g) and the re-excitation of the electron from the defect to the CBM (processes-j and k). However, since the defect levels are located far away from the CBM and much closer to the VBM as shown in Figure 3, the processes of electron re-excite to CBM can be safely ignored due to the large energy jump dE (the energy differences between the defect levels and the CBM or VBM) needed in such a process. The processes of electron transition from CBM to defect and hole

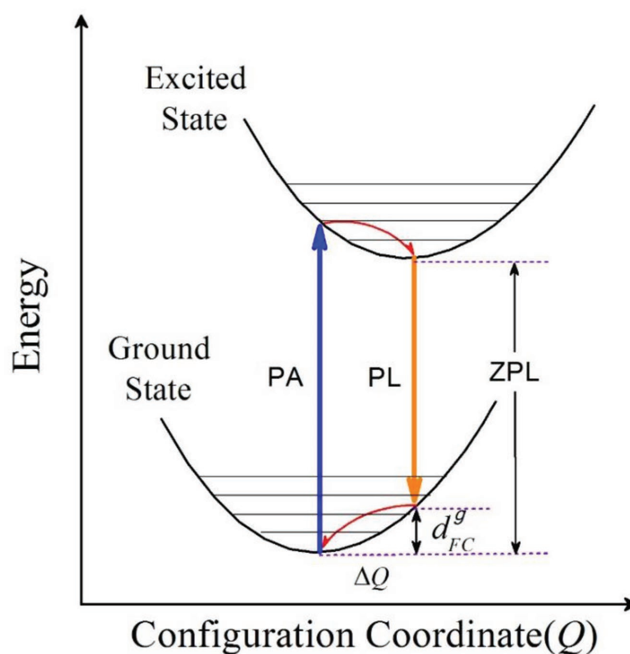

Figure 2. The configuration coordinate diagram shows a series of defect-related photophysical process. **PA** is an excited process from ground state to excited state and **PL** is a de-excited process from excited state to ground state. The **ZPL** is also represented in the diagram.

© 2017 WILEY-VCH Verlag GmbH & Co. KGaA, Weinheim

ADVANCED OPTICAL MATERIALS
www.advopticalmat.de

Table 1. Calculated photoabsorption (PA) and photoluminescence (PL) energies and zero phonon line (ZPL), and transition energies (ΔE) of defects C_N and C_N+O_N using the HSE hybrid functional.

Defect	Transition level		E_{PA} [eV]	E_{PL} [eV]	ZPL [eV]	ΔE [eV]
C_N	−/0	Theory[14]	2.95	2.14	2.6	0.81
		Theory[18]	2.81	1.98	2.45	1.04
		Theory[27]	3.04	2.18	2.67	0.78
		This work	3.01	2.16	2.71	0.79
C_N+O_N	0/+	Theory[16]	3.30	2.25	2.70	0.75
		Theory[27]	3.13	2.28	2.77	0.66
		This work	3.11	2.23	2.74	0.76
Experiment		[16]	3.32	2.20	2.60	0.85
		[7]	3.19	2.15	2.64 ± 0.05	0.86
		[21]		2.22	2.59	0.916

transition from VBM to defect contain both RR and non-RR, but with very different energy dependence. The non-RR process needs phonon participation, while the RR process does not. According to Equation (21) of ref. [30], the non-RR has an exponential decay dependence on dE (the energy jump), while Equation (1) of ref. [38] reveals that the RR is proportional to dE. Thus, while the RR efficiency increases with dE, the non-RR efficiency decreases rapidly with dE. As a result, in our following discussion, we will only consider the RR processes for the electron transitions from CBM to defect levels, and non-RR processes for the hole transitions between VBM and defect levels. This will be further justified in our calculation later. Note that, in order to simplify the model, the other competing channels (including the common visible luminescence and other unknown nonradiative recombination channels) are not shown in Figure 3. However, their effects to the YL emission have been rolled into the hole concentration which we deduced from the experimental band edge emission density.

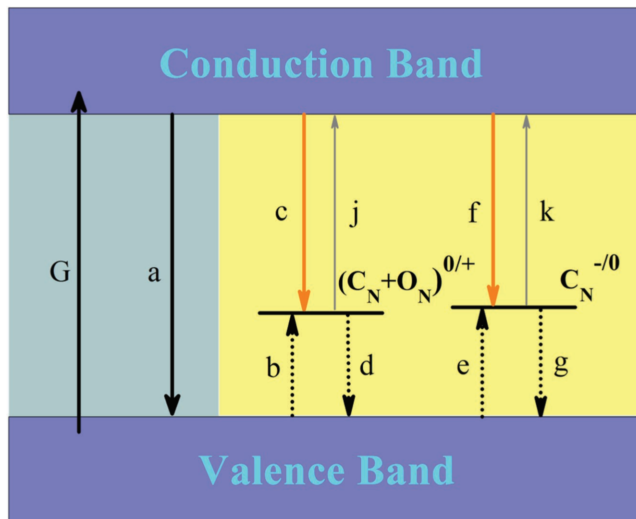

Figure 3. Diagram to show the relevant excitation and recombination processes in GaN containing C_N+O_N and C_N defects.

All the other channels can have a role in determining this hole concentration.

The steady-state equation for concentration of neutral defect complex C_N+O_N (N^0_{YL1}) is then expressed as

$$\frac{dN^0_{YL1}}{dt} = -C_{YL1}\, N^0_{YL1} p + N^+_{YL1}/\tau_{YL1} + Q_{YL1}\, N^+_{YL1} = 0 \tag{1}$$

Here, $C_{YL1}N^0_{YL1}p$ is the hole non-RR (process-b) rate for holes being captured by neutral defect complex C_N+O_N, where C_{YL1} is the hole non-RR coefficient for 0/+ process and p is the concentration of free holes in the valence band. N^+_{YL1}/τ_{YL1} is the electron RR (process-c) rate, where N^+_{YL1} is the concentration of the defect complex C_N+O_N at charge "+" state and τ_{YL1} is the lifetime of the defect at "+" due to 0/+ transition of electron fall into N^+_{YL1} (YL1 emission). τ_{YL1} depends on electron majority carrier concentration, as well as the photoemission oscillator strength between CBM and the defect state. $Q_{YL1}N^0_{YL1}$ is the hole re-excitation (process-d) rate from impurity level to VBM. (the C_N+O_N from "+" to neutral for a hole to jump from the defect state to the VBM). The coefficient Q_{YL1} of thermal activation of holes is related to the capture coefficient C_{YL1} through a detail balance[11]

$$Q_{YL1} = C_{YL1}\, N_v g^{-1} \exp\left(-\frac{\Delta E}{kT}\right) \tag{2}$$

with

$$N_v = 2\left(\frac{m_h k_B T}{2\pi\hbar^2}\right)^{3/2} \tag{3}$$

where g is the degeneracy factor of the acceptor level, N_v is the effective density of states in the valence band, and ΔE is the transition energy (0.76 eV).

Similarly, the steady-state equation for concentration of defect C_N at "−" charge state (N^-_{YL2}) is then similarly expressed as

$$\frac{dN^-_{YL2}}{dt} = -C_{YL2}\, N^-_{YL2} p + N^0_{YL2}/\tau_{YL2} + Q_{YL2}\, N^0_{YL2} = 0 \tag{4}$$

Here, C_{YL2} is the hole non-RR coefficient for YL2, and τ_{YL2} is the lifetime of the N^-_{YL2} defect due to electron photoemission from CBM to the defect state (YL2 emission). Q_{YL2} is the coefficient of hole thermal activation for N^0_{YL2} (hole jumping from N^0_{YL2} to VBM), and the corresponding transition energy is 0.79 eV. Here, the sum of N^0_{YL1} and N^+_{YL1} is the concentration of the defect complex C_N+O_N, and N^-_{YL2} plus N^0_{YL2} is the concentration of defect C_N. We then have

$$N_{YL1} = N^0_{YL1} + N^+_{YL1};\; N_{YL2} = N^-_{YL2} + N^0_{YL2} \tag{5}$$

The hole non-RR coefficients C_{YL1}, C_{YL2}, lifetime of electrons for YL1 (τ_{YL1}) and YL2 (τ_{YL2}) will be obtained in this study. The above transition rates depend on the free carrier concentration. In an n-type system, while the concentration of the majority electron carrier can be considered as a constant, the minority hole (p) concentration will depend on excitation G, the channels discussed above, as well as many other possible channels

© 2017 WILEY-VCH Verlag GmbH & Co. KGaA, Weinheim

undiscussed (e.g., the band edge RR channel and other unknown non-RR channels). At this stage, we are still unable to include all the other channels to pin down the hole concentration p for a given G and temperature. Fortunately, the temperature-dependent hole concentration is directly proportional to band edge luminescence, which can be measured experimentally. The QE of band edge luminescence can be represented as

$$\eta_{\text{free}}(T) = \frac{C_{\text{free}} np}{G} \tag{6}$$

where C_{free} is the free carrier photoemission recombination coefficient and it has been obtained from pure ab initio calculation. The detailed procedure is presented in Section 4.

We thus use this information to get the concentration p. After taking into account all the above, we can get the temperature-dependent concentrations of recombination center N^0_{YL1}, N^+_{YL1}, N^-_{YL2}, and N^0_{YL2} using Equations (1), (2), (4), and (5), respectively. These are nonlinear equations, but they can be solved numerically relatively easily.

Finally, we can get the QE expressions for YL1 and YL2 as

$$\eta_{\text{YL1}}(T) = \frac{N^+_{\text{YL1}}}{G\tau_{\text{YL1}}} \tag{7}$$

$$\eta_{\text{YL2}}(T) = \frac{N^0_{\text{YL2}}}{G\tau_{\text{YL2}}} \tag{8}$$

If an electron is in an excited state, it may spontaneously decay to the ground state, at the same time, releasing the energy difference as a photon. The radiative rate between two states can be described by Fermi's golden rule[38,39] the concrete form of which is given by

$$W_{\text{rad}}(\omega) = \frac{\omega^3 n|\mu_{ij}|^2}{3\pi\varepsilon_0 \hbar c^3} = \frac{4\alpha\omega^3 n|\langle i|r|j\rangle|^2}{3c^2} = \frac{4\alpha\omega^3 n|\langle i|p|j\rangle|^2}{3c^2} \times \frac{\hbar^2}{\Delta E_{ij}^2 m_e^2}$$
$$\frac{|\mu_{ij}|^2}{\pi\varepsilon_0 \hbar c} = 4\alpha|\langle i|r|j\rangle|^2 = 4\alpha|\langle i|p|j\rangle|^2 \times \frac{\hbar^2}{\Delta E_{ij}^2 m_e^2} \tag{9}$$

where ω is the emission frequency, n is the index of refraction, μ_{ij} is the transition dipole moment, ε_0 is the vacuum permittivity, $\hbar$ is the reduced Planck constant, c is the vacuum speed of light, α is the fine structure constant, ΔE_{ij} is the difference between these two energy states, r is the position operator, and p is the momentum operator.

For the processes of a, c, and f in Figure 3, the phonon-assisted non-RR can be ignored due to the large energy difference between defect levels and CBM. The above Equation (9) was employed to calculate the recombination rates of progresses of a, c, and f. For emission frequency $\omega = {}^{2\pi c}/_{\lambda}$, the corresponding ΔE_{ij} of the band-edge, YL1 and YL2 processes are 3.50, 2.23, and 2.16 eV. The initial state i is always chosen as CBM, and the j states are VBM, $(C_N{+}O_N)^+$, and C^0_N, respectively. The impurity state wave functions of $(C_N{+}O_N)^+$ and C^0_N are localized in a 128-atom supercell as illustrated in **Figure 4**. The calculated results are listed in **Table 2**. In our case, the formula of radiation recombination coefficient is $C_n = W_{\text{rad}} \times V$ (V is the volume of the supercell which is equal to 1.48×10^{-21} cm^3), and then we can use $\tau_n = 1/(C_n \times n)$ to get electron lifetime. n is the concentration of free electrons, including the concentrations of intrinsic (n_0) and photogenerated (δn). At low excitation intensity condition ($n_0 \gg \delta n$) in our simulation, we have $n \approx n_0$, and the value is taken as 2.8×10^{17} cm^{-3} according to Table IV of ref. [9]. We have treated the n-type majority electron carrier concentration (n) as independent of temperature. Since the experimental n-doping defect binding energy is unknown, treating the n temperature dependent can only complicate the analysis. After this, the calculated radiation recombination coefficients of free carrier (C_{free}), YL1 and YL2 bands are 4.24×10^{-9}, 5.22×10^{-13}, and 3.16×10^{-13} cm^3 s^{-1}, and the electron lifetime are 3.37×10^{-10}, 6.84×10^{-6}, and 1.13×10^{-5} s, respectively. Unfortunately, the value C_{free} in the literature is not completely settled either from experiments or theory. For example, refs. [40–42] give this coefficient as 2.0×10^{-11} cm^3 s^{-1}, while refs. [43,44] give this coefficient as 1.1×10^{-8} cm^3 s^{-1}, all at room temperature. Our calculated value is in between.

For the hole captured processes of b and e in Figure 3, the calculated RR coefficients are very small, about 10^{-14} cm^3 s^{-1}.

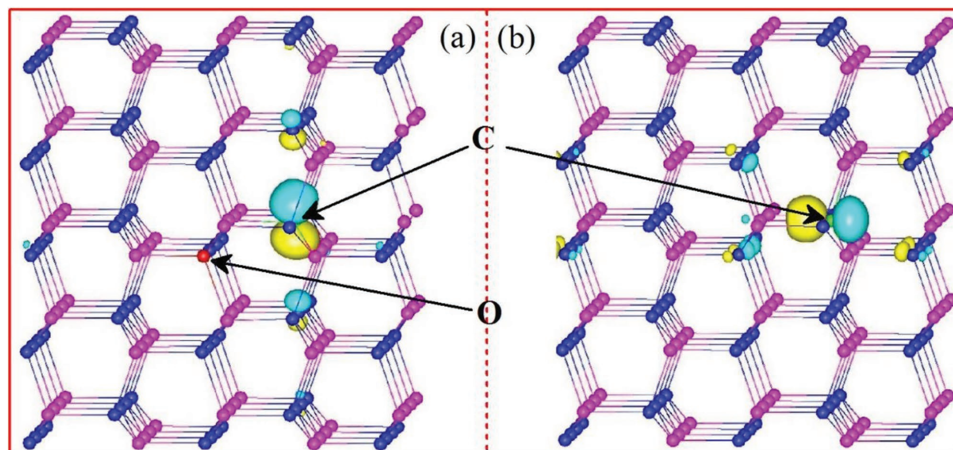

Figure 4. The square of wavefunctions of impurity levels of $(C_N{+}O_N)^+$, and C^0_N in the 128-atom supercell calculated using the HSE DFT function. The yellow is a negative isosurface of impurity wavefunctions while the cyan is a positive isosurface.

© 2017 WILEY-VCH Verlag GmbH & Co. KGaA, Weinheim

Table 2. The calculation results of radiative recombination (RR) of defects C_N, C_N+O_N, and intrinsic transition using Equation (9).

	CBM-VBM	C_N+O_N(0/+)	C_N (−/0)
ΔE_{ij}	3.5 eV	2.23 eV	2.16 eV
$\langle i\|p\|f\rangle^2$	0.43	0.08	0.05
W_{rad} [s^{-1}]	2.97×10^9	3.53×10^8	2.14×10^8
C_n [cm^3 s^{-1}]$^{a)}$	4.24×10^{-9}	5.22×10^{-13}	3.16×10^{-13}
τ [s]$^{b)}$	3.37×10^{-10}	6.84×10^{-6}	1.13×10^{-5}

$^{a)}C_n = W_{rad} \times V$; $^{b)}\tau_n = 1/(C_n \times n)$.

It means that these transitions must be phonon related. For the phonon-induced nonradiative carrier recombination processes, the relevant electron–phonon coupling should be between the impurity states and the VBM states. Then we used a combined dynamic matrix (CDM) method as described in ref. [29] to calculate the phonon modes and phonon DOSs. Here, we used R_c (= 7.2 a.u.), for which the CDM describes well the impurity DOS.[29] The results are shown in **Figure 5**, one can see some new phonon-mode peaks localized within the gap and at high energy end of bulk phonon DOS. From the calculated phonon frequency (ω_k) and eigenvector $\mu_k(R)$ of every phonon mode, as well as the atomic displacement (K_k) after the electron charge transfer, and the electron–phonon coupling constant ($C^k_{i,j}$), we calculated the nonradiative decay probability W_{ij} using state coupling formulas. The detailed formalism can be found in our previous publications.[30] The capture coefficient can be calculated via $C_p = W_{ij} \cdot V$. The results are shown in **Figure 6**. At T = 600 K, we get $C_{YL1} = 5.1 \times 10^{-7}$ cm^3 s^{-1}, and the C_{YL2} is calculated as 3.9×10^{-7} cm^3 s^{-1}, which agree well with the experimental fitted value 3–6 × 10^{-7} cm^3 s^{-1}.[16,45] However, the experimental fitting values use parameters which do not change with temperature, while our calculated coefficients vary significantly with temperature. The above agreements only hold near the temperature before the quench of YL. Thus,

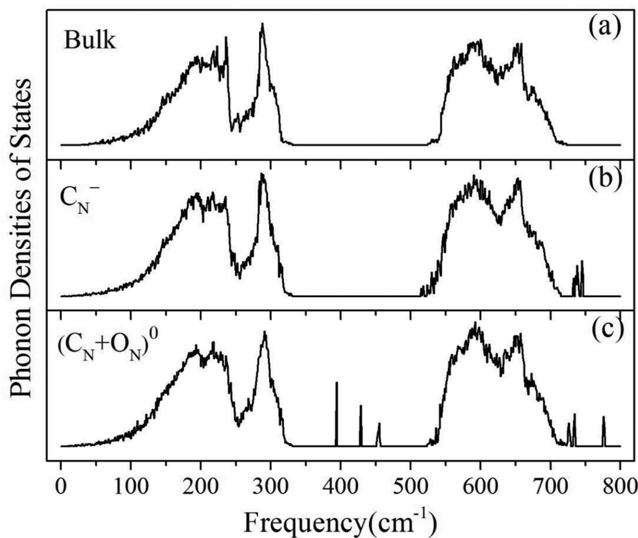

Figure 5. The phonon densities for GaN bulk, C_N^-, and $(C_N+O_N)^0$ in 128-atom supercell.

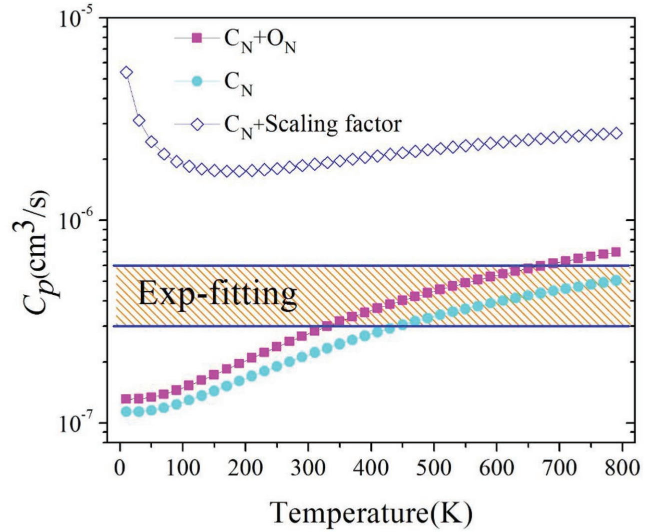

Figure 6. Calculated nonradiative and radiative hole capture rates C_p at the C_N and C_N+O_N defects in GaN. The shaded parts represent the experimental data from refs. [9,16]. The hollow diamonds represent the "scaling factor" corrected nonradiative hole capture rates of C_N.

for a more accurate comparison, the temperature dependence should be included. Furthermore, since the nonradiative carrier recombination process of C_N is from "−" to "0," in the actual experimental system, before the transition, the concentration of holes close to the electronegative defect (C_N^-) has a higher concentration than its average value. In other words, the hole spends more time near the defect due to Coulomb attraction. Previous works have introduced a correction "scaling factor" $f(T)$ to describe this effect.[17,46] The formula is expressed as: $C_p = f(T)\widetilde{C_p} = \frac{C}{T^{1/2}}\widetilde{C_p}$, where $\widetilde{C_p}$ is the coefficient before the correction, and C is a constant determined numerically. For the nonradiative carrier recombination process of C_N in our work, we adopted $C \approx 150$ K$^{1/2}$ following ref. [17]. The corrected nonradiative carrier recombination coefficients are shown in Figure 6, which are in the range of a few 10^{-6} cm^3 s^{-1}. Because there are no long-range Coulomb interactions between the neutral defect and the hole, as reported in the case of GaN:(Zn_{Ga}-V_N), the calculated scaling factor is f = 1.05,[17] and we thus ignored such a factor in the PL process of the C_N+O_N defect.

With the hole non-RR coefficients C_{YL1}, C_{YL2}, lifetime of electrons for YL1 (τ_{YL1}) and YL2 (τ_{YL2}) have all been obtained, we next employ Equation (2) to get the holes re-excite rates from $(C_N+O_N)^+$ and C_N^- to VBM as shown in Figure 3 (process-d and process-g), and the transition energies (ΔE) are 0.76 and 0.79 eV, respectively, and g = 2, $N_v = 3.2 \times 10^{15}$ T$^{3/2}$ cm^{-3} are adopted for GaN following refs. [9,18]. The band edge luminescence has been observed experimentally in the samples containing YL band.[9] In Figure 5 of ref. [9], the QE of a total emission in the range 3.3–3.5 eV (called "exciton band" in ref. [9]) is presented. We know that this energy range actually includes both the contribution of exciton and band edge luminescence. Since most excitons are dissociated at room temperatures, we can consider this QE purely as from band edge luminescence. Combined with the known electron

© 2017 WILEY-VCH Verlag GmbH & Co. KGaA, Weinheim

concentration (n) and the free carrier photoemission recombination coefficient (C_{free}), we can employ Equation (6) to get the temperature-dependent hole concentration (p). The shape of the p curve is same as the QE curve of band edge luminescence, and the concentrations are about 10^6 cm^{-3}. Here, the electron–hole pair generation rate (G = 3.0×10^{19} cm^{-3} s^{-1}) was adopted. This is taken from experiment value according to their laser intensity and absorption coefficient.[9] As mentioned in the Introduction, the concentrations of C and O will vary widely among different samples. We then take a wide range of 2.0×10^{15}–2.0×10^{18} cm^{-3} for the defect concentrations for both C_N and C_N+O_N for the purpose of comparison. All the above numbers can be plugged in Equations (1), (2), (4), and (5) to yield a steady-state solution. From these, we can get the temperature and defect concentration-dependent QE of YL emission using Equations (7) and (8), and the results are shown in **Figure** 7a,b. The defect concentration will only affect the scale of the QE and will not change the overall trend. As the defect concentrations decrease, the QE of YL1 and YL2 are gradually reduced at given temperature, while their quenching temperatures are unchanged. The overall trends of both YL1 and YL2 are consistent with the experiment.[9] As shown in Figure 7a, the YL1 is consistent with the experimental results when the concentration of defect C_N+O_N is 1.0×10^{18} cm^{-3}, while Figure 7b shows that when the concentration of defect C_N is 2.0×10^{17} cm^{-3}, its YL2 is consistent with experiments.

We then use a larger value $n = 7.0 \times 10^{17}$ cm^{-3} in order to test the effect of electron concentration. The temperature-dependent QE of YL1 and YL2 are shown in Figure 7c,d. Obviously, the YL1 and YL2 are still in good agreement with the experiments when the defect concentrations are 1.0×10^{18} cm^{-3} (for C_N+O_N) and 2.0×10^{17} cm^{-3} (for C_N), respectively. This shows the final result is not very sensitive to the electron carrier concentration. This is because when n is higher, using Equation (6) and the experimentally observed band edge emission $\eta_{free}(T)$, and the obtained hole concentration p will be smaller. Because of that, the $(C_N+O_N)^+$ and C_N^0 will be smaller. This cancels out the increased n in the YL emission formula, and yield similar emission strength as before. Thus, our result is relatively robust against the electron concentration.

It is interesting to see the competition between different channels for a given defect. As shown in **Figure 8**, we present the temperature-dependent RR, non-RR, and hole thermal activation rates of defect C_N ($n = 7.0 \times 10^{17}$ cm^{-3} and $N_{YL1} = 2.0 \times 10^{17}$ cm^{-3}). While the non-RR create the C_N^0 state, the RR and the hole thermal activation from the defect bring it back to the C_N^- state. Thus, the sum of RR and hole thermal activation equal to the rate of non-RR. The defect captured holes at low temperature will not be thermally activated to the valence band. Most holes will be combined with the electrons to emit YL. As the thermal activation rate increases exponentially with temperature, after about 480 K, the rate of thermal activation becomes larger than the RR, and the RR is quenched

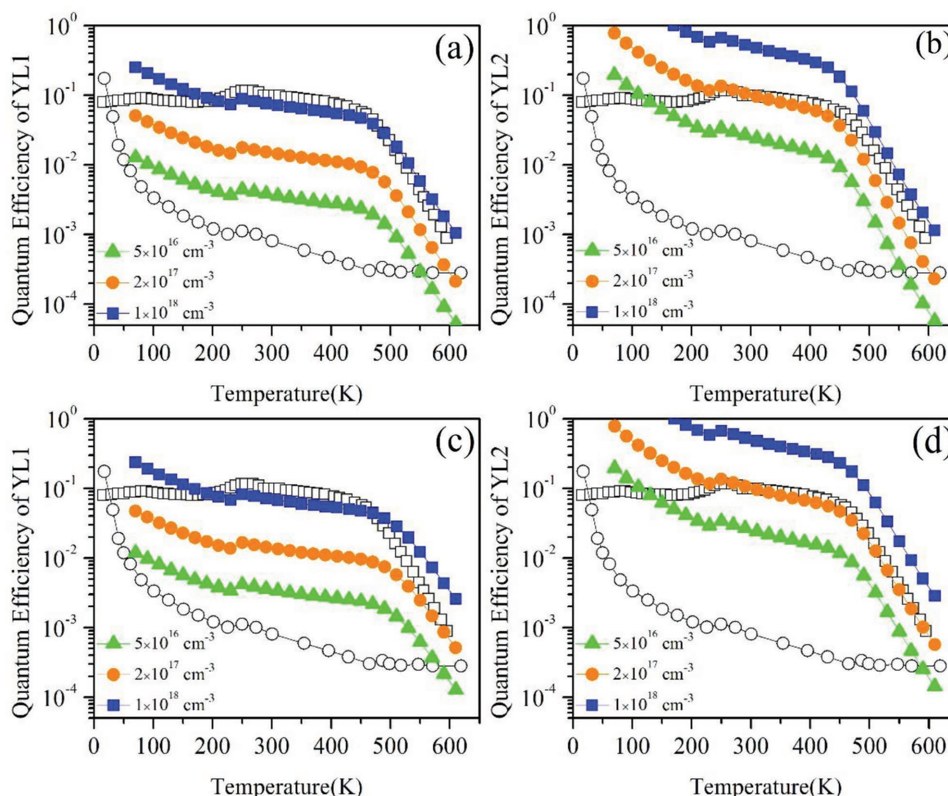

Figure 7. Calculated QE of YL1 and YL2 under different defect concentrations (N_i). The excitation intensity that we adopted is G = 3.0×10^{19} cm^{-3} s^{-1}. The concentrations of electrons are taken: a,b) 2.8×10^{17} cm^{-3} and c,d) 7.0×10^{17} cm^{-3}, respectively. The hollow circles and diamonds are experimental values of exciton and YL bands citing from Figure 5 of ref. [9].

© 2017 WILEY-VCH Verlag GmbH & Co. KGaA, Weinheim

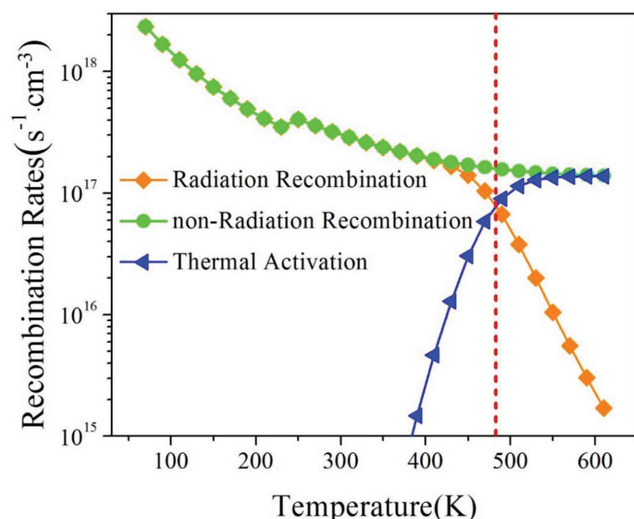

Figure 8. The temperature-dependent recombination rates of radiation, nonradiation, and thermal activation of point defect C_N. The vertical red dotted line indicates that the processes radiation recombination and thermal activation have the same recombination rates at that temperature.

due to the lack of C_N^0 charge state. Surprisingly, the non-RR rate is relatively smooth across the 480 K threshold.

In summary, we propose a practical approach to study the quantum efficiency of point defect-related photoluminescence, combining experimental optical measurements with ab initio calculations. We use the YL band in GaN as an example. Based on our DFT energetics calculation, we propose that YL1 and YL2 (correspond to PL transitions from $(C_N+O_N)^+$ to $(C_N+O_N)^0$ and from C_N^0 to C_N^-, respectively) are possible candidates for the experimentally observed YL. Via calculating the relevant radiation and non-RR processes, we obtain the temperature dependences of the quantum efficiency of YL1 and YL2. The YL1 and YL2 are consistent with the experiment when the concentrations of C_N+O_N and C_N are 1.0×10^{18} and 2.0×10^{17} cm^{-3}, respectively. Further studies might be necessary, for example, with better determination of the defect concentrations, to more definitely identify the defect type as the origin of the YL. We expect that our approach can be applied widely to understand the microscopic under pining of optical spectroscopy of point defects in semiconductors.

Acknowledgements

L.S. was supported by the National Natural Science Foundation of China (Grant No. 11374328), the National Key Research and Development Program of China (Grant Nos. 2016YFA0201101 and 2016YFE0105700), the National Science Fund for Distinguished Young Scholars (Grant No. 61325022), the Youth Innovation Promotion Association Chinese Academy of Science (CAS) (Grant No. 2016289), and the Foundation of Suzhou Institute of Nano-Tech and Nano-Bionics (SINANO) (Grant No. Y5AAC11001). L.-W.W. was supported by the Director, Office of Science (SC), Basic Energy Science (BES), Materials Science and Engineering Division (MSED), of the U.S. Department of Energy (DOE) under Contract No. DE-AC02-05CH11231 through the Material Theory Program (KC2301). The authors are grateful for the professional services offered by the Platforms of Characterization & Test at SINANO, and Supercomputing Center, CNIC, CAS.

Conflict of Interest

The authors declare no conflict of interest.

Keywords

quantum efficiencies, DFT calculations, point defects, III-V semiconductors, radiation recombination, non-radiation recombination

Received: April 28, 2017
Revised: July 26, 2017
Published online: September 12, 2017

[1] R. Dingle, M. Ilegems, *Solid State Commun.* **1971**, *9*, 175.
[2] R. Dingle, D. D. Sell, S. E. Stokowski, M. Ilegems, *Phys. Rev. B* **1971**, *4*, 1211.
[3] B. Monemar, *Phys. Rev. B* **1974**, *10*, 676.
[4] A. Isamu, A. Hiroshi, *Jpn. J. Appl. Phys.* **1997**, *36*, 5393.
[5] Y. Dora, A. Chakraborty, L. Mccarthy, S. Keller, S. P. Denbaars, U. K. Mishra, *IEEE Electron Device Lett.* **2006**, *27*, 713.
[6] M. A. Reshchikov, M. Z. Iqbal, H. Morkoç, S. S. Park, K. Y. Lee, *Appl. Phys. Lett.* **2003**, *83*, 266.
[7] O. Toshio, A. Masaharu, *Jpn. J. Appl. Phys.* **1980**, *19*, 2395.
[8] D. M. Hofmann, D. Kovalev, G. Steude, B. K. Meyer, A. Hoffmann, L. Eckey, R. Heitz, T. Detchprom, H. Amano, I. Akasaki, *Phys. Rev. B* **1995**, *52*, 16702.
[9] M. A. Reshchikov, R. Y. Korotkov, *Phys. Rev. B* **2001**, *64*, 115205.
[10] H. Z. Xu, A. Bell, Z. G. Wang, Y. Okada, M. Kawabe, I. Harrison, C. T. Foxon, *J. Cryst. Growth* **2001**, *222*, 96.
[11] M. A. Reshchikov, H. Morkoç, S. S. Park, K. Y. Lee, *Appl. Phys. Lett.* **2002**, *81*, 4970.
[12] R. Armitage, W. Hong, Q. Yang, H. Feick, J. Gebauer, E. R. Weber, S. Hautakangas, K. Saarinen, *Appl. Phys. Lett.* **2003**, *82*, 3457.
[13] R. Y. Korotkov, M. A. Reshchikov, B. W. Wessels, *Phys. B* **2003**, *325*, 1.
[14] J. L. Lyons, A. Janotti, C. G. Van de Walle, *Appl. Phys. Lett.* **2010**, *97*, 152108.
[15] M. A. Reshchikov, H. Morkoç, S. S. Park, K. Y. Lee, *Mater. Res. Soc. Symp. Proc.* **2001**, *693*, I6.19.
[16] D. O. Demchenko, I. C. Diallo, M. A. Reshchikov, *Phys. Rev. Lett.* **2013**, *110*, 087404.
[17] A. Alkauskas, Q. Yan, C. G. Van de Walle, *Phys. Rev. B* **2014**, *90*, 075202.
[18] M. A. Reshchikov, D. O. Demchenko, A. Usikov, H. Helava, Y. Makarov, *Phys. Rev. B* **2014**, *90*, 235203.
[19] Q. Wang, Y. Liu, Y. Sun, Y. Tong, G. Zhang, *J. Semicond.* **2016**, *37*, 083001.
[20] W. Götz, L. T. Romano, B. S. Krusor, N. M. Johnson, R. J. Molnar, *Appl. Phys. Lett.* **1996**, *69*, 242.
[21] M. A. Reshchikov, J. D. McNamara, F. Zhang, M. Monavarian, A. Usikov, H. Helava, Y. Makarov, H. Morkoç, *Phys. Rev. B* **2016**, *94*, 035201.
[22] A. Armstrong, A. R. Arehart, D. Green, U. K. Mishra, J. S. Speck, S. A. Ringel, *J. Appl. Phys.* **2005**, *98*, 053704.
[23] G. A. Slack, L. J. Schowalter, D. Morelli, J. A. Freitas, *J. Cryst. Growth* **2002**, *246*, 287.
[24] M. A. Reshchikov, A. A. Kvasov, M. F. Bishop, T. McMullen, A. Usikov, V. Soukhoveev, V. A. Dmitriev, *Phys. Rev. B* **2011**, *84*, 075212.
[25] D. O. Demchenko, I. C. Diallo, M. A. Reshchikov, *J. Appl. Phys.* **2016**, *119*, 035702.

© 2017 WILEY-VCH Verlag GmbH & Co. KGaA, Weinheim

[26] Q. Yan, P. Rinke, M. Scheffler, C. G. Van de Walle, *Appl. Phys. Lett.* **2009**, *95*, 121111.
[27] S. G. Christenson, W. Xie, Y. Y. Sun, S. B. Zhang, *J. Appl. Phys.* **2015**, *118*, 135708.
[28] J. L. Lyons, A. Alkauskas, A. Janotti, C. G. Van de Walle, *Phys. Status Solidi* **2015**, *252*, 900.
[29] L. Shi, L.-W. Wang, *Phys. Rev. Lett.* **2012**, *109*, 245501.
[30] L. Shi, K. Xu, L.-W. Wang, *Phys. Rev. B* **2015**, *91*, 205315.
[31] G. Kresse, J. Hafner, *Phys. Rev. B* **1993**, *47*, 558.
[32] G. Kresse, J. Furthmüller, *Phys. Rev. B* **1996**, *54*, 11169.
[33] W. Jia, Z. Cao, L. Wang, J. Fu, X. Chi, W. Gao, L.-W. Wang, *Comput. Phys. Commun.* **2013**, *184*, 9.
[34] W. Jia, J. Fu, Z. Cao, L. Wang, X. Chi, W. Gao, L.-W. Wang, *J. Comput. Phys.* **2013**, *251*, 102.
[35] J. Heyd, G. E. Scuseria, M. Ernzerhof, *J. Chem. Phys.* **2003**, *118*, 8207.
[36] O. Madelung, *Semiconductors: Basic Data*, 2nd ed., Springer, Berlin, Germany **1996**.
[37] S.-H. Wei, *Comput. Mater. Sci.* **2004**, *30*, 337.
[38] A. F. van Driel, G. Allan, C. Delerue, P. Lodahl, W. L. Vos, D. Vanmaekelbergh, *Phys. Rev. Lett.* **2005**, *95*, 236804.
[39] G. I. B. Henderson, *Optical Spectroscopy of Inorganic Solids*, Clarendon, Oxford, UK **1989**.
[40] J. S. Im, A. Moritz, F. Steuber, V. Härle, F. Scholz, A. Hangleiter, *Appl. Phys. Lett.* **1997**, *70*, 631.
[41] A. Dmitriev, A. Oruzheinikov, *J. Appl. Phys.* **1999**, *86*, 3241.
[42] T. Malinauskas, K. Jarašiūnas, R. Aleksiejunas, D. Gogova, B. Monemar, B. Beaumont, P. Gibart, *Phys. Status Solidi* **2006**, *243*, 1426.
[43] F. Binet, J. Y. Duboz, E. Rosencher, F. Scholz, V. Härle, *Appl. Phys. Lett.* **1996**, *69*, 1202.
[44] J. F. Muth, J. H. Lee, I. K. Shmagin, R. M. Kolbas, H. C. Casey, B. P. Keller, U. K. Mishra, S. P. DenBaars, *Appl. Phys. Lett.* **1997**, *71*, 2572.
[45] M. A. Reshchikov, H. Morkoç, *J. Appl. Phys.* **2005**, *97*, 061301.
[46] R. Pässler, *Phys. Status Solidi* **1976**, *78*, 625.

© 2017 WILEY-VCH Verlag GmbH & Co. KGaA, Weinheim